

Bulletin of the Seismological Society of America

This copy is for distribution only by
the authors of the article and their institutions
in accordance with the Open Access Policy of the
Seismological Society of America.

For more information see the publications section
of the SSA website at www.seismosoc.org



THE SEISMOLOGICAL SOCIETY OF AMERICA
400 Evelyn Ave., Suite 201
Albany, CA 94706-1375
(510) 525-5474; FAX (510) 525-7204
www.seismosoc.org

CAN-HK: An a Priori Crustal Model for the Canadian Shield

by D. A. Thompson, J.-M. Kendall, G. R. Helffrich, I. D. Bastow, J. Wookey, and D. B. Snyder

Online Material: Tables of the crustal model and Generic Mapping Tools-compatible files, and color versions of figures.

INTRODUCTION

Crustal structure, which can vary greatly over relatively short length scales depending on the tectonic setting, has the potential to significantly influence the data used to infer the deeper features of the Earth. In particular, commonly implemented teleseismic methods are sensitive to crustal velocity structure but are invariably incapable of resolving it. Moho depth has a first-order effect on travel-time residuals of teleseismic body waves (> 1 s variation; e.g., Waldhauser *et al.*, 2002); and, for typical Rayleigh-wave periods of < 150 s, the crust can contribute 50% or more to the surface-wave-derived velocity variations (Ritsema *et al.*, 2004; Artemieva, 2011). Crustal structure can also significantly affect the correct extraction of radial anisotropy in surface-wave studies (Ferreira *et al.*, 2010; Panning *et al.*, 2010). The use of a high-resolution crustal model thus has the potential to markedly enhance studies of the mantle.

There are a number of global crustal models in circulation, for instance CRUST5.1 (Mooney *et al.*, 1998), CRUST2.0 (Bassin *et al.*, 2000), and CRUST1.0 (Laske *et al.*, 2013). These may lack the resolution required for detailed local seismic studies, especially where there are significant lateral variations in crustal structure across short length scales (e.g., at ocean–continent transitions; Marone and Romanowicz, 2007). Moreover, global compilations often require assumptions regarding local geology to extrapolate structure to regions of poor coverage.

The goal of this contribution is to present a unified 3D crustal model of the Canadian shield. The new model presented here, CAN-HK, utilizes new passive broadband deployments in the region (Eaton *et al.*, 2005; Bastow, Kendall, *et al.*, 2011; Bastow *et al.*, 2015). For several key tectonic features of the Canadian shield (Fig. 1), CAN-HK shows striking deviations in crustal thickness (> 10 km) and predicted teleseismic body-wave travel times (up to 1.5 s) compared to CRUST1.0. CAN-HK can thus be used either as part of a regional starting model or as a crustal correction for a variety of studies from the crust to upper and lower mantle. The model is particularly apposite because the footprint of the Transportable Array com-

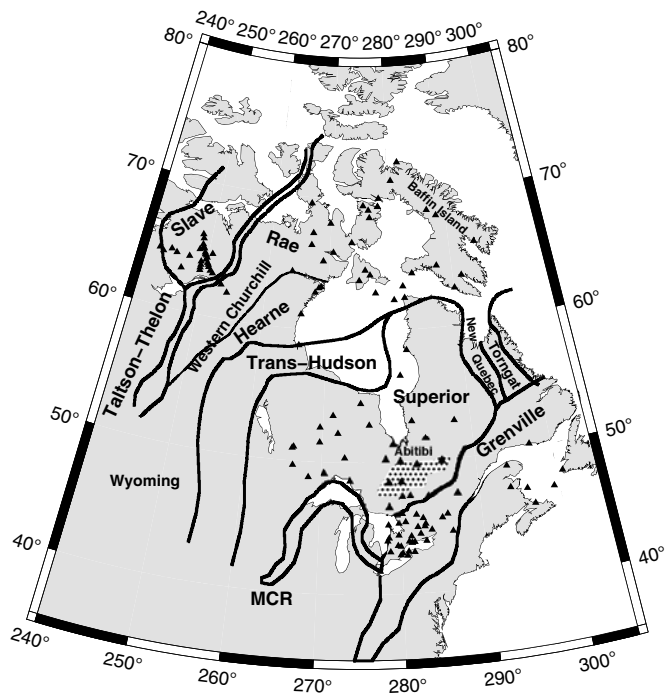
ponent of USArray is adjacent to, and in places overlapping with, our study region. The model can therefore be incorporated into detailed, continent-wide investigations of the whole of North America.

DATA AND METHOD

We combine broadband seismic data from the Portable Observatories for Lithospheric Analysis and Research Investigating Seismicity (POLARIS) network (Eaton *et al.*, 2005), the Canadian High Arctic Seismic Monitoring Experiment (CHASME; Darbyshire, 2003), and the Canadian National Seismic Network (CNSN). Data from temporary deployments associated with the Hudson Bay Lithospheric Experiment (HuBLE) (e.g., Thompson *et al.*, 2010, 2011; Bastow, Kendall, *et al.*, 2011; Bastow, Thompson, *et al.*, 2011; Pawlak *et al.*, 2011; Steffen *et al.*, 2012; Bastow *et al.*, 2015) are also used. In total, 134 broadband seismic stations contribute to the CAN-HK crustal model, providing unparalleled coverage and resolution for the Canadian shield (Fig. 1). The results presented in this study are all new measurements performed in a uniform manner, removing potential bias from amalgamating the results of previous studies using differing processing flows or parameters.

Receiver functions (RFs) are produced using the extended time multitaper approach of Helffrich (2006) with a low-pass \cos^2 taper that is equal to zero above 1 Hz. After RFs were visually inspected to check for signal causality and instances of unstable deconvolution were removed, a total of 7175 make up the final dataset.

The H – κ stacking method (Zhu and Kanamori, 2000), a simple and commonly used technique for determining crustal properties, is implemented to determine the thickness (H) and bulk V_p/V_s ratio (κ). The method involves a grid search over plausible values of H and V_p/V_s for a layer over a half-space, stacking amplitude along predicted moveout curves for the direct Moho P_s phase and subsequent reverberations ($PpPs$ and $PpPs + PsPs$; Fig. 2) using all data from a given station. The parameters that provide the best fit to the data lead to a maximum in stacking amplitude. Results in this study assume a crustal V_p of 6.5 km/s, a common value for cratonic studies

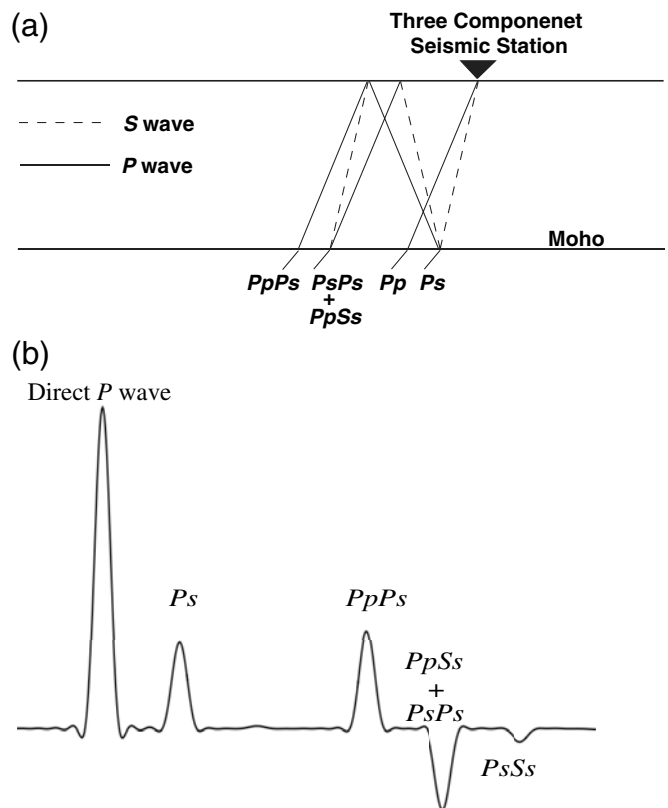


▲ **Figure 1.** Key tectonic features of the Canadian shield, including Archean crustal domains (Slave, Rae, Hearne, and Superior, including the Abitibi Greenstone belt, Wyoming), Proterozoic orogens (Trans-Hudson, Taltson-Thelon, New Quebec, Torngat, Grenville) and the Mid-Continent rift (MCR). Triangles are the broadband seismic stations incorporated into the CAN-HK model.

such as this (e.g., Nair *et al.*, 2006; Thompson *et al.*, 2010), with amplitudes being stacked linearly along predicted move-out curves using weights of 0.5, 0.3, and 0.2 for the P_s , $PpPs$, and $PpSs + PsPs$, respectively (Zhu and Kanamori, 2000; Thompson *et al.*, 2010). Models produced with a range of assumed crustal P -wave velocities (6.3–6.7 km/s) and with different weights (0.7, 0.2, and 0.1) are also provided (see [Electronic Supplement](#) to this article). These results can be combined to form different models if required, but we prefer to present results with a uniform crustal V_p .

Because of the remote nature of the stations producing little cultural noise and the low attenuating characteristics of cratons in general, data quality is excellent and the $H-\kappa$ results obtained from the data are particularly well constrained. The method employed and subsequent models accurately match the travel times of the crustal seismic phases, both direct (P_s) and multiply reverberated phases ($PpPs$ and $PpSs + PsPs$); this can be seen clearly in the stacked RFs for each station in Figure 3. This validates the fact that CAN-HK can provide accurate crustal travel-time corrections for both P and S waves at typical teleseismic slownesses and that the results are robust.

Point estimates of crustal thickness and V_p/V_s ratio for each station are used to produce a smoothed surface defined every 1° laterally using the Generic Mapping Tools (GMT; Wessel and Smith, 1995). All models are provided both as plain text files and GMT-compatible grid files (see [Electronic Supplement](#) to this article).



▲ **Figure 2.** (a) Simplified ray diagram of crustal phases used in the $H-\kappa$ stacking method. (b) Schematic receiver function for the simple crustal model.

RESULTS

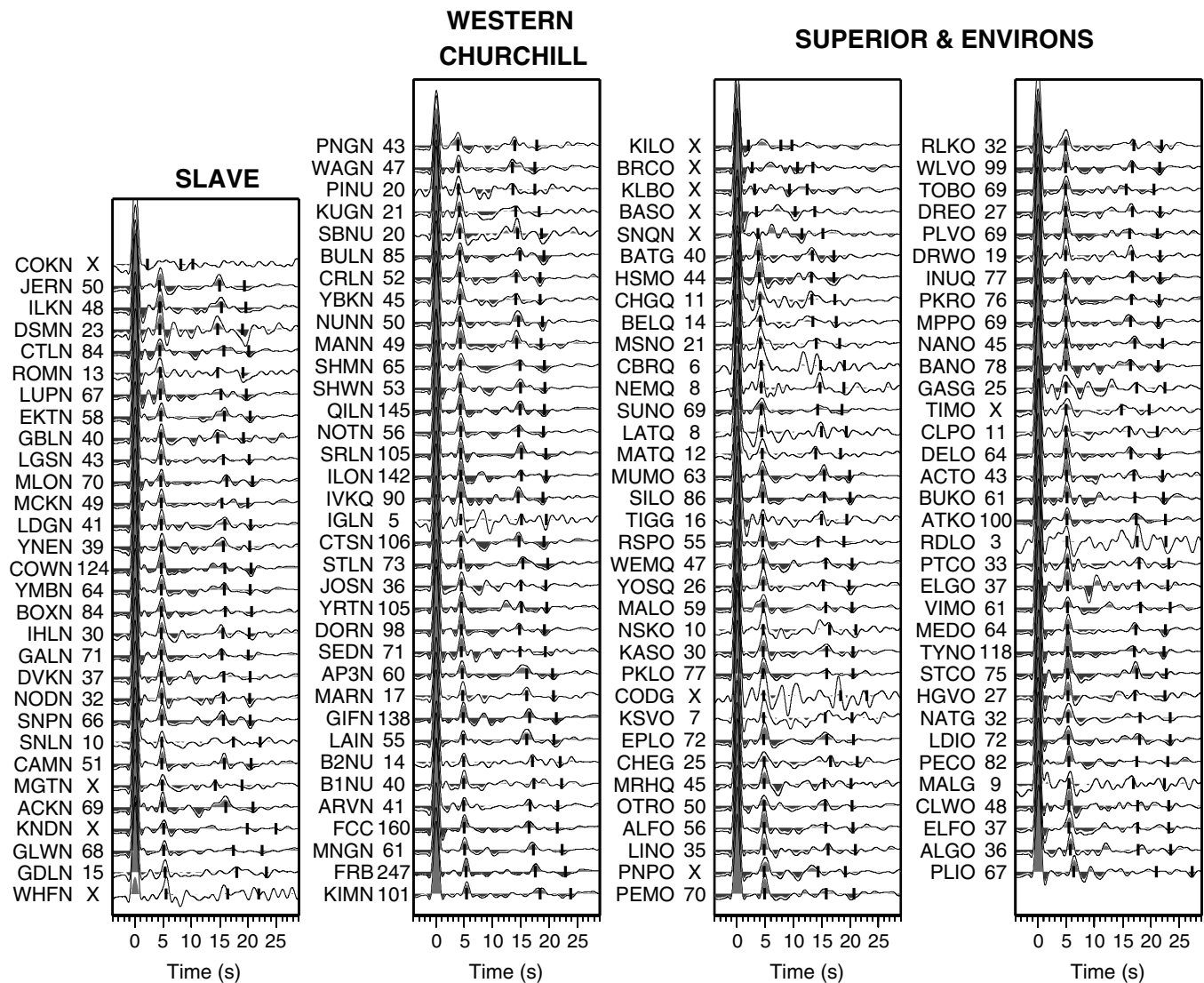
CAN-HK Features

Western Churchill Craton

The $H-\kappa$ results for the Western Churchill craton have been presented previously by Thompson *et al.* (2010). Distinct variations in both crustal thickness and V_p/V_s ratio were observed across several crustal subdomains of the northern Hudson Bay region. The thickest crust (~ 43 km) is seen beneath central and southern Baffin Island; and whereas the crust of the Western Churchill is of relatively uniform thickness (~ 37 km), contrasts in V_p/V_s ratio can be seen between the Hearne domain (> 1.75) and the Rae domain (< 1.73). These results suggest a secular change in crustal formation processes from nonplate tectonic prior to 3.0 Ga toward fully developed plate tectonics at 1.8 Ga. See Thompson *et al.* (2010) for a more in-depth discussion on the implications and variability of crustal structure in the northern Hudson Bay region.

Slave Craton

Previous estimates of crustal thickness from within the Slave craton show a northwest–southeast pattern, with a thickening trend from ~ 37 km in the northwest to ~ 42 km in the southeast (Bank *et al.*, 2000; Davis *et al.*, 2003). A similar pattern is also evident from the new estimates of crustal thickness



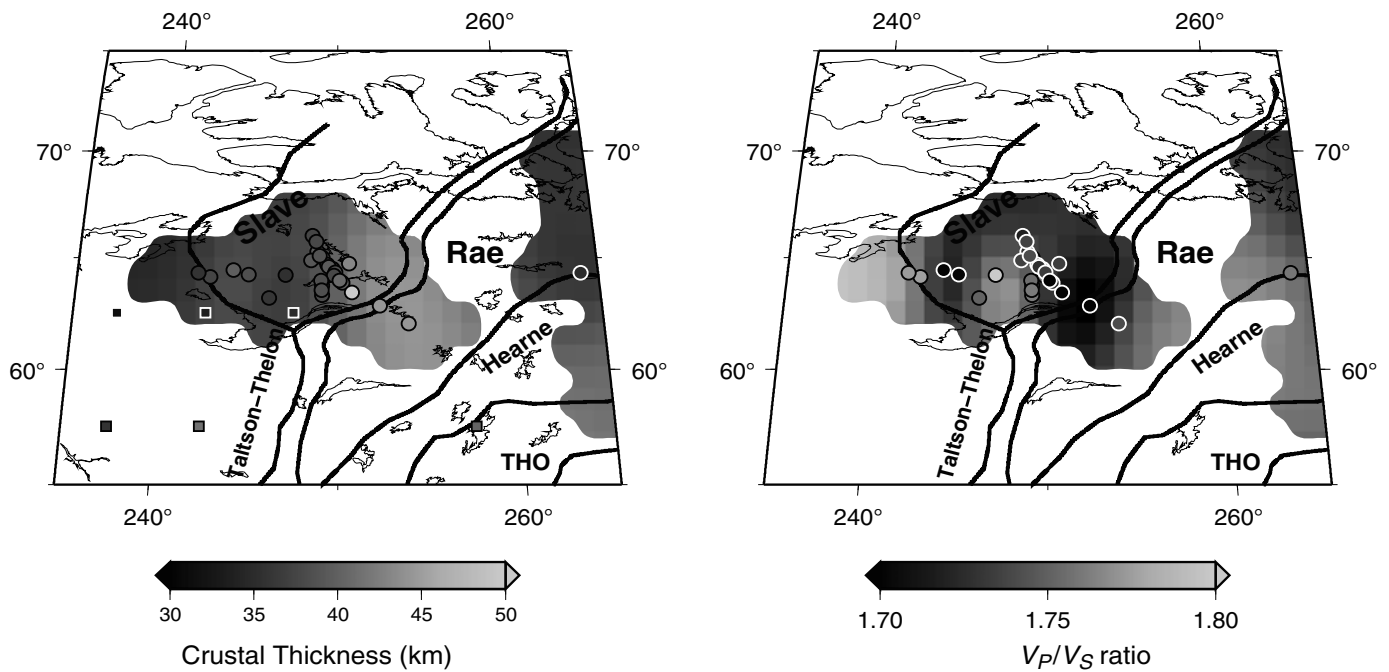
▲ **Figure 3.** Stacked receiver functions for each of the stations used in the study grouped by region and plotted in ascending order with respect to the predicted arrival time of the Moho P_s phase. Black lines are the stacked traces, and only amplitudes above the 2σ confidence limit are plotted. The number associated with each station is the number of receiver functions contributing to the stacks; stations that were removed from the final crustal model are labeled with an X in place of the number of receiver functions. The predicted arrival times of the three crustal phases determined using the best-fitting H and V_p/V_s ratio for each station are labeled on each trace using short vertical lines. All stations used in the final model have excellent agreement between the data and predicted times from the model, highlighting the fact that the CAN-HK model can accurately predict body-wave travel times within the crust for typical teleseismic slownesses. © A color version of this figure is available as Figure S1 in the electronic supplement.

presented here (Fig. 4). Mean crustal thickness is 39.1 km across the Slave craton, consistent with the previous studies. The crustal thickness estimates provided here are also in good agreement with constraints from Lithoprobe active source experiments (LITH5.0; Perry *et al.*, 2002). Previous crustal thickness estimates were based purely on controlled-source P -wave observations or on the arrival time of the Moho P_s phase without taking into account the reverberated phases. Hence, the bulk V_p/V_s ratio results presented here are some of the first for the Slave craton. The mean V_p/V_s ratio is 1.738, typical for cratonic crust in general due to it lying below the continental

average (1.768; Christensen, 1996). The northwest–southeast pattern present in the crustal thickness does not appear to manifest itself strongly in the V_p/V_s ratios, although some of the lowest V_p/V_s ratios (<1.72) do lie toward the southeast of the Slave network (Fig. 4).

Superior Craton and Environs

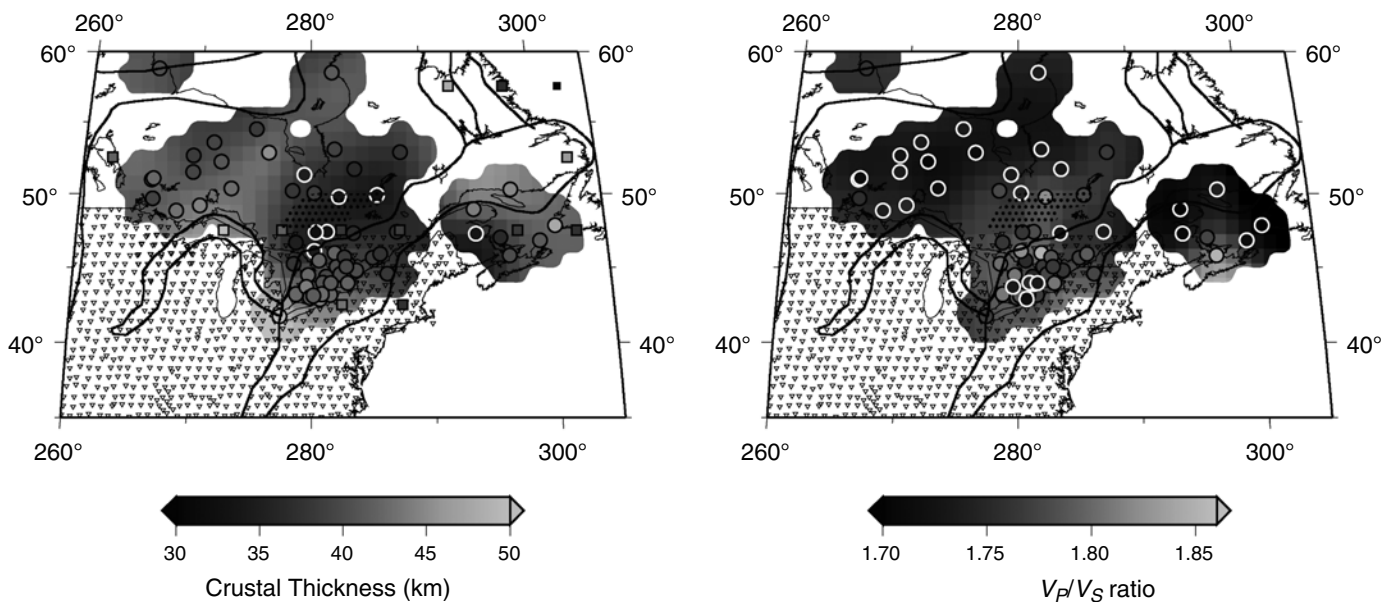
Significant variations in both crustal thickness and V_p/V_s ratio are evident from within the Superior craton itself and its adjacent geological terranes (Fig. 5; Grenville orogen, Appalachian orogen, Kapuskasing structural zone, Keweenawan



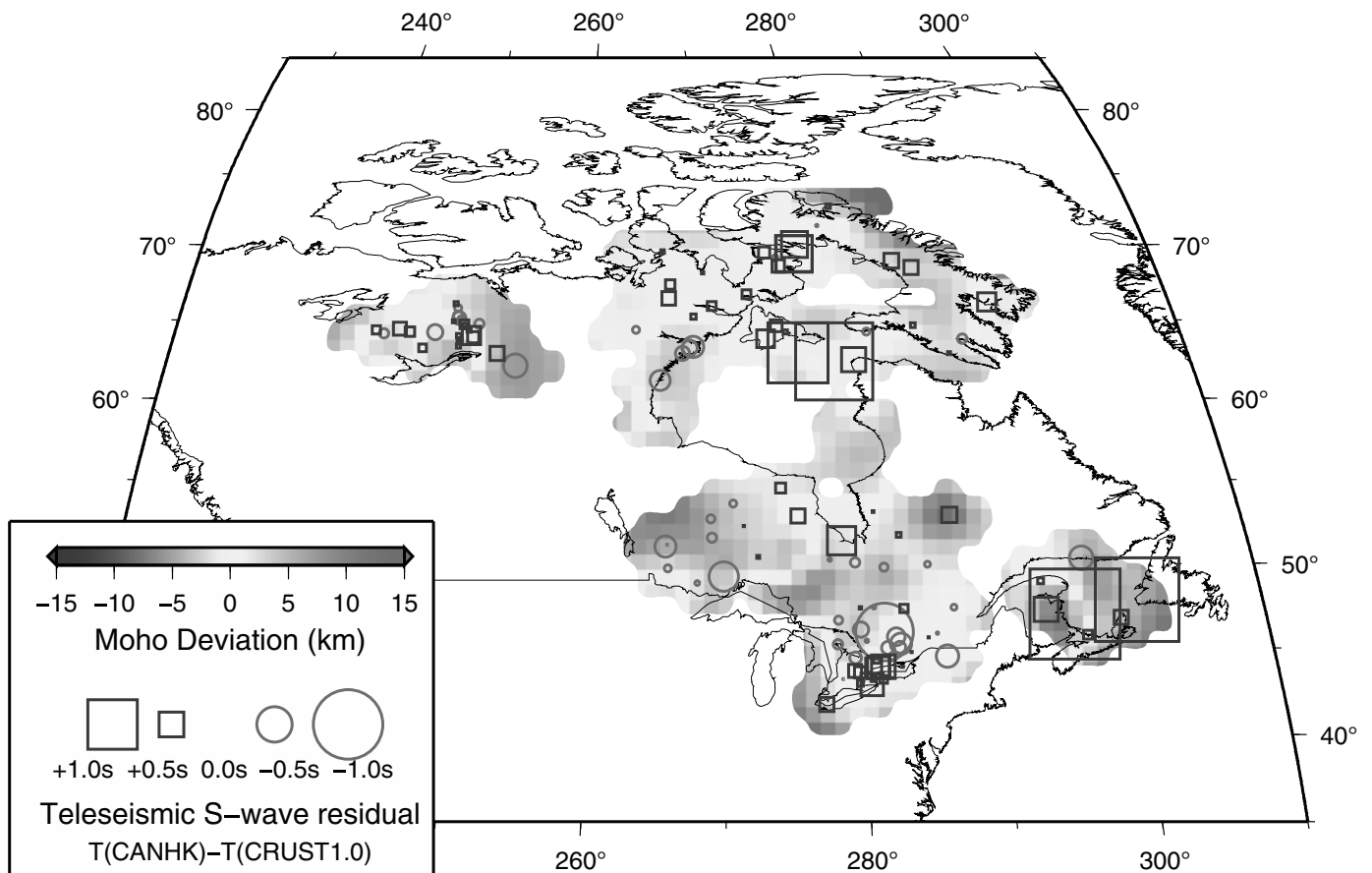
▲ **Figure 4.** Results from the $H-\kappa$ stacking analysis for the Slave craton. Filled circles are the point estimates from individual stations (stations with crustal thickness of below 35 km or with a $V_p = V_s$ ratio < 1.75 are drawn with a white line, black line otherwise) and the backgrounds are the $1.0^\circ \times 1.0^\circ$ interpolated surfaces from the CAN-HK model. (left) Crustal thickness with filled squares being the crustal thickness estimates from the LITH5.0 crustal model (Perry *et al.*, 2002). (right) V_p/V_s ratio. THO, Trans-Hudson orogen. © A color version of this figure is available as Figure S2.

midcontinent rift). Eaton *et al.* (2006) and Darbyshire *et al.* (2007) presented results using a version of the $H-\kappa$ method modified to include semblance-weighted stacking for the Superior region. Crustal thickness varied from ~ 34 to ~ 44 km

across most of the region, with anomalously thick crust (~ 44 km) in the region of the Kapuskasing structural zone. The V_p/V_s ratio also correlates well with regional geology, elevated values (> 1.80) being associated with areas expected



▲ **Figure 5.** Results from the $H-\kappa$ stacking analysis for the Superior craton region. Geological terranes are the same as those plotted in Figure 1. Plotting convention follows Figure 4, except that the triangles are USArray stations. © A color version of this figure is available as Figure S3.



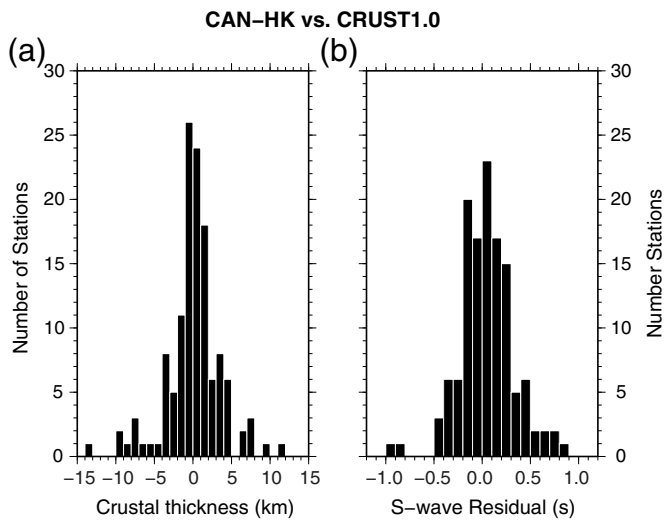
▲ **Figure 6.** Comparison of the CAN-HK and CRUST1.0 models. The background shading is the difference between the CAN-HK and CRUST1.0 crustal thicknesses. The symbols show differences in teleseismic S -wave travel time measured at each seismic station. The ak135 model (Kennett *et al.*, 1995) is used for travel-time calculation, except that at depths between the Moho and 210 km the V_P and V_S are equal to those at 210 km, mimicking the largely uniform velocities through the cratonic lithosphere (Eaton *et al.*, 2009). © A color version of this figure is available as Figure S4.

to have a greater mafic component throughout the crust (i.e., regions affected by continental rifting or within the Abitibi Greenstone belt; Figs. 1 and 5). The patterns observed in this study using the linear $H-\kappa$ method are broadly consistent with the findings of the Eaton *et al.* (2006) and Darbyshire *et al.* (2007). The results are also in agreement with data from the Teleseismic Western Superior Transect (TWiST) experiment, in which crustal thickness estimates range from 38 to 47 km (Angus *et al.*, 2009), and also the LITH5.0 model of Perry *et al.* (2002). Stations in the Superior subset from this study exhibit a mean crustal thickness of 39.9 km, with values ranging between 32 and 45 km. Thicker crust (> 40 km) appears to be associated with either Proterozoic orogeny (Grenville orogen) or the midcontinent rift (Fig. 5). The mean V_P/V_S ratio is elevated compared to the Slave and Rae domains at 1.758, but it is identical to the Hearne domain, which, much like the Superior craton, exhibits widespread granite-and-greenstone geology (Thompson *et al.*, 2010). As in previous studies, the highest values (> 1.80) appear to be associated with the Abitibi Greenstone belt, the Keweenaw midcontinent rift, and

the Central Gneiss belt of the Grenville orogen (exhumed lower crustal rocks; Eaton *et al.*, 2006; Darbyshire *et al.*, 2007). Away from these areas, the V_P/V_S ratio is comparatively low (< 1.75), typical of felsic-to-intermediate cratonic crust.

Comparison with CRUST1.0

CRUST1.0 (Laske *et al.*, 2013), the latest global model providing estimates of crustal thickness and velocity structure at 1° intervals, is currently the highest resolution compilation available. The model incorporates crustal thickness estimates from previous active and passive-source seismic experiments; and, where these constraints are unavailable, gravity measurements are used (Laske *et al.*, 2013). In regions where the CAN-HK model has good data coverage, CRUST1.0 is also defined by previous seismic experiments. Despite this, significant discrepancies in crustal thickness remain (Fig. 6). Where the crust is at its thinnest within the Superior Province, the deviation from CRUST1.0 is as much 10 km (Fig. 6). Across the majority of the Slave domain, deviations from CRUST1.0 are less than 5 km.



▲ **Figure 7.** Differences in (a) crustal thickness ($H(\text{CAN} - \text{HK}) - H(\text{CRUST1.0})$) and (b) teleseismic S -wave residual ($T_S(\text{CAN} - \text{HK}) - T_S(\text{CRUST1.0})$). The S -wave residual skewness suggests slightly larger predicted CAN-HK residuals.

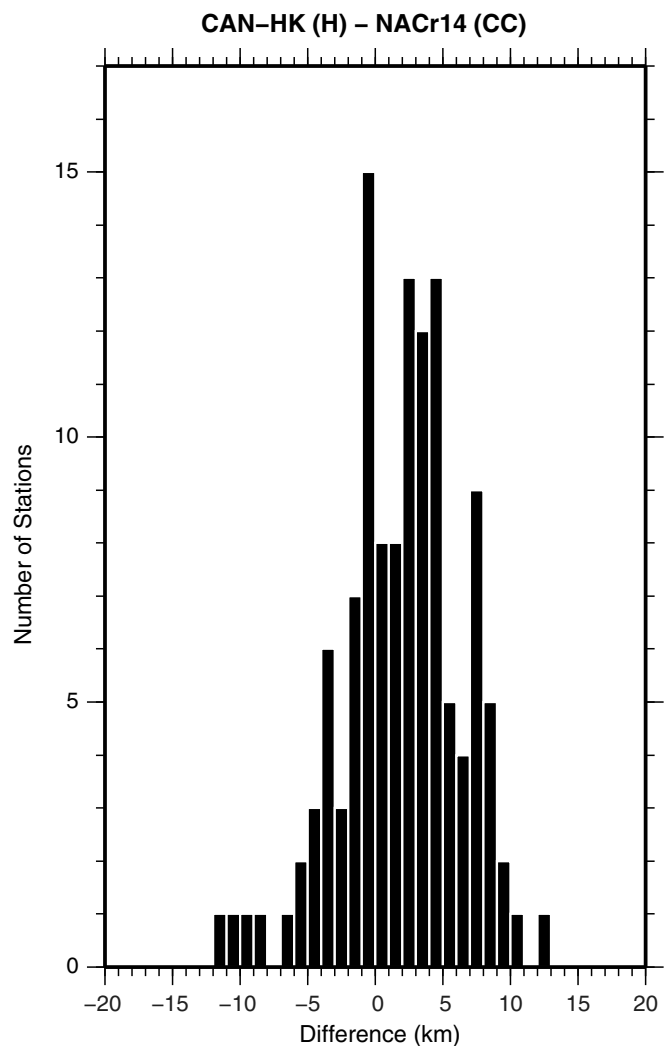
The only exception to this is the very southeast of the network, where CAN-HK crustal thicknesses lie ~ 7 km thicker.

Differences in S -wave travel time at each seismic station incorporated into this study between the CAN-HK model and the nearest grid point of the CRUST1.0 model, assuming uniform Earth structure beneath the crust, are also plotted in Figure 6. Any discrepancy in S -wave arrival time between the two models would mean that different crustal corrections would be derived depending on the choice of model. Figure 6 shows that differences in the S -wave travel time from a deep teleseismic event (410 km depth, 65° distance) can be as high as 1 s (Crotwell *et al.*, 1999). This is significant because previous studies of the Canadian shield have found travel-time residuals on the order of ± 2.5 s (e.g., Frederiksen *et al.*, 2001). Histograms showing the differences between the models are shown in Figure 7. Incorrect crustal correction could therefore contaminate mantle structure in body-wave tomographic inversions and also lead to incorrect mapping of energy to depth in migration-based seismic techniques.

The parameters provided in the CAN-HK model are inherently dependent on the choice of bulk crustal V_p . Variations in crustal thickness for reasonable estimates of V_p (our chosen range of 6.3–6.7 km/s) are on the order of ± 2 km from our preferred value of 6.5 km/s, meaning that deviations from CRUST1.0 are relatively insensitive to the assigned value of this parameter (see   the electronic supplement).

Comparison with Continental Scale Studies

New crustal models, herein referred to as the Kao13 and NACr14 models, respectively, for the North American continent have been recently presented by Kao *et al.* (2013) and Tesauro *et al.* (2014). The Kao13 model is an S -wave velocity model produced using ambient noise observations, whereas the

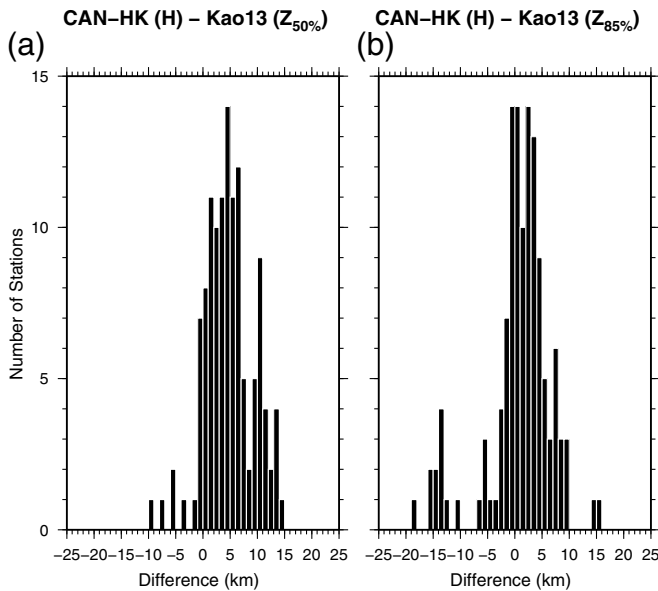


▲ **Figure 8.** Differences between crustal thickness from the CAN-HK model and the thickness of the crystalline crust (CC) from the NACr14 model (Tesauro *et al.*, 2014). The skewness suggests slightly larger CAN-HK crustal thicknesses.

NACr14 model is a P -wave velocity model that uses the U.S. Geological Survey crustal structure database.

In Figure 8, the variations between the point estimates of crustal thickness from each station derived in this study are compared with the thickness of the crystalline crust at the closest node provided in the NACr14 model. As with CRUST1.0, many of the stations lie within 5 km of the NACr14 estimate (Fig. 8). However, there are certain stations that again exhibit significant deviations (10 km or greater).

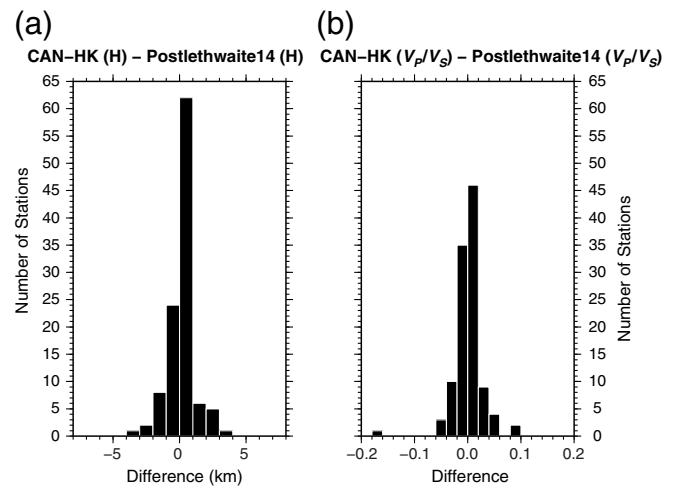
Comparison with two parameters from the Kao13 model are shown in Figure 9 (the 50% and 85% increase in V_S between the lower crust and mantle, $Z_{50\%}$ and $Z_{85\%}$, respectively; Kao *et al.*, 2013). Almost all the values in Figure 9a lie above 0 km, indicating that $Z_{50\%}$ lies consistently shallower than our crustal thickness estimates. As expected, $Z_{85\%}$ values lie closer to the CAN-HK crustal thickness estimates; $Z_{85\%}$ values also lie closer to crustal thickness estimates from CRUST1.0, a feature that



▲ **Figure 9.** Differences between crustal thickness from the CAN-HK model and (a) depth to 50% of the velocity increase from the lower crust to mantle ($Z_{50\%}$) and (b) depth to 85% of the velocity increase from the lower crust to mantle ($Z_{85\%}$) from [Kao et al. \(2013\)](#). The uniformly thicker CAN-HK predictions are shown by the ~ 5 km offsets in the $Z_{50\%}$ comparison, whereas bimodality in the $Z_{85\%}$ comparison suggests coherent small-scale upper-mantle architectures beneath the southeast Superior/Grenville orogen region.

[Kao et al. \(2013\)](#) uses to justify $Z_{85\%}$ as representing the depth to the ambient noise Moho. Also evident in [Figure 9b](#) is a subset of stations that are centered at -15 km (i.e., $Z_{85\%}$ is 15 km deeper than the CAN-HK crustal thickness). Stations in this subset are centered in the southeast Superior Province and the Grenville orogen (see [Figs. 1 and 5](#)). It is intriguing that spatially coherent discrepancies occur beneath these stations given the high-quality nature of the data used in this study. We speculate that this subset, not clearly observed in the $Z_{50\%}$ comparison, may well be associated with heterogeneous shallow lithospheric mantle structure, potentially creating complex increases in S -wave velocity in the top 100 km. This may be in the form of anisotropy ([Levin and Park, 2000](#)), a Hales discontinuity ([Hales, 1969](#); [Lebedev et al., 2009](#)), or the recently observed Mid-Lithospheric discontinuity ([Abt et al., 2010](#)).

A recent study by [Postlethwaite et al. \(2014\)](#) of the entire Canadian landmass provides estimates of crustal thickness and V_p/V_s ratio using a different variant of the H - κ approach to that used here (semblance-weighted stacking; [Eaton et al., 2006](#)). Also different from the approach used for CAN-HK (which provides a range of assumed V_p values), [Postlethwaite et al. \(2014\)](#) elect to use a single average value from the nearest 1° node of the CRUST1.0 model. [Figure 10](#) shows the differences in H and V_p/V_s ratio for concurrent stations. All crustal thickness estimates lie within 5 km of each other, with most stations having a discrepancy of less than 1 km. Similarly, the V_p/V_s ratios are also very close (most stations



▲ **Figure 10.** Differences in (a) crustal thickness and (b) V_p/V_s ratio between the single station CAN-HK results and those from [Postlethwaite et al. \(2014\)](#).

varying by less than 0.05, although some outliers exceed this). Given that many of the same stations are incorporated into these two studies, and the similarity between data analysis techniques, it is unsurprising and reassuring that the single station results from CAN-HK are in good agreement with those of [Postlethwaite et al. \(2014\)](#).

CONCLUDING REMARKS

A new, unified *a priori* crustal model (CAN-HK) has been produced for the Canadian shield. The model provides comprehensive data coverage for the Canadian shield by incorporating constraints from several passive-source seismic initiatives. Noteworthy and consistent variations in both crustal thickness and bulk crustal V_p/V_s ratio are evident across several key tectonic features of the North American continent. Predicted teleseismic body-wave travel-time residuals between CAN-HK and CRUST1.0 can be as much as ~ 1 s. In addition to this, significant (~ 10 km) deviations in crustal thickness between existing global and continental scale models exist across the Superior craton and its adjacent terranes. CAN-HK can be used as a starting model to more detailed crustal investigation or as correction for larger scale, lower frequency studies.

DATA AND RESOURCES

Portable Observatories for Lithospheric Analysis and Research Investigating Seismicity (POLARIS), Canadian High Arctic Seismic Monitoring Experiment (CHASME), and Canadian National Seismograph Network (CNSN) data were obtained through the Natural Resources Canada autodrm service (http://www.earthquakescanada.nrcan.gc.ca/stdon/AutoDRM/autodrm_req-eng.php; last accessed June 2010). Data from the temporary Hudson Bay Lithospheric Experiment (HuBLE)

seismic deployment will be available through Incorporated Research Institutions for Seismology in 2016. ✉

ACKNOWLEDGMENTS

The United Kingdom component of the Hudson Bay Lithospheric Experiment (HuBLE) was supported by the Natural Environment Research Council (NERC) Grant Number NE/F007337/1, with financial and logistical support from the Geological Survey of Canada (GSC), Canada-Nunavut Geoscience Office (CNGO), SEIS-UK (the seismic node of NERC), and the First Nations communities of Nunavut. J. Beauchesne and J. Kendall provided invaluable assistance in the field. I. D. B. was funded by the Leverhulme Trust and acknowledges support through Grant Number RPG-2013-332. The authors thank three anonymous reviewers for their constructive comments.

REFERENCES

- Abt, D. L., K. M. Fischer, S. W. French, H. A. Ford, H. Yuan, and B. Romanowicz (2010). North American lithospheric discontinuity structure imaged by P_S and S_P receiver functions, *J. Geophys. Res.* **115**, no. B09301, 1–24.
- Angus, D. A., J.-M. Kendall, D. C. Wilson, D. J. White, S. Sol, and C. J. Thomson (2009). Stratigraphy of the Archean western Superior Province from P - and S -wave receiver functions: Further evidence for tectonic accretion? *Phys. Earth Planet. In.* **177**, nos. 3/4, 206–216, doi: [10.1016/j.pepi.2009.09.002](https://doi.org/10.1016/j.pepi.2009.09.002).
- Artemieva, I. M. (2011). *The Lithosphere: An Interdisciplinary Approach*, Cambridge University Press, Cambridge, United Kingdom.
- Bank, C. G., M. G. Bostock, R. M. Ellis, and J. F. Cassidy (2000). A reconnaissance teleseismic study of the upper mantle and transition zone beneath the Archean Slave craton in NW Canada, *Tectonophysics* **319**, no. 3, 151–166.
- Bassin, C., G. Laske, and T. G. Masters (2000). The current limits of resolution for surface wave tomography in North America, *Eos Trans. AGU* **81**, F897.
- Bastow, I. D., D. W. Eaton, J.-M. Kendall, G. Helffrich, D. B. Snyder, D. A. Thompson, J. Wookey, F. A. Darbyshire, and A. Pawlak (2015). The Hudson Bay Lithospheric Experiment (HuBLE): Insights in Precambrian plate tectonics and the development of mantle keels, in *Continent Formation Through Time*, N. M. W. Roberts, M. Van Kranendonk, S. Parman, S. Shirey, and P. D. Clift (Editors), Geological Society, London, Special Publications, Vol. 389, 41–67, doi: [10.1144/SP389.7](https://doi.org/10.1144/SP389.7).
- Bastow, I. D., J.-M. Kendall, A. M. Brisbourne, D. B. Snyder, D. A. Thompson, D. Hawthorne, G. Helffrich, J. Wookey, and D. W. Eaton (2011). The Hudson Bay Lithospheric Experiment: A remote success in Arctic Canada, *Astron. Geophys.* **52**, no. 6, 6.21–6.24, doi: [10.1111/j.1468-4004.2011.52621.x](https://doi.org/10.1111/j.1468-4004.2011.52621.x).
- Bastow, I. D., D. A. Thompson, J. Wookey, J.-M. Kendall, G. Helffrich, D. B. Snyder, D. W. Eaton, and F. A. Darbyshire (2011). Precambrian plate tectonics: Seismic evidence from northern Hudson Bay, Canada, *Geology* **39**, no. 1, 91–94, doi: [10.1130/G31396.1](https://doi.org/10.1130/G31396.1).
- Christensen, N. I. (1996). Poisson's ratio and crustal seismology, *J. Geophys. Res.* **101**, no. B2, 3139–3156.
- Crotwell, H. P., T. J. Owens, and J. Ritsema (1999). The TauP toolkit: Flexible seismic travel-time and ray-path utilities, *Seismol. Res. Lett.* **70**, no. 2, 154–160, doi: [10.1785/gssrl.70.2.154](https://doi.org/10.1785/gssrl.70.2.154).
- Darbyshire, F. A. (2003). Crustal structure across the Canadian High Arctic region from teleseismic receiver function analysis, *Geophys. J. Int.* **152**, no. 2, 372–391.
- Darbyshire, F. A., D. W. Eaton, A. W. Frederiksen, and L. Ertolahti (2007). New insights into the lithosphere beneath the Superior Province from Rayleigh wave dispersion and receiver function analysis, *Geophys. J. Int.* **169**, 1043–1068, doi: [10.1111/j.1365-246X.2006.03259.x](https://doi.org/10.1111/j.1365-246X.2006.03259.x).
- Davis, W. J., A. G. Jones, W. Bleeker, and H. Grütter (2003). Lithosphere development in the Slave craton: A linked crustal and mantle perspective, *Lithosphere* **71**, no. 2, 575–589.
- Eaton, D. W., J. Adams, I. Asudeh, G. M. Atkinson, M. G. Bostock, J. F. Cassidy, I. J. Ferguson, C. Samson, D. B. Snyder, K. F. Tiampo, and M. J. Unsworth (2005). Investigating Canada's lithosphere and earthquake hazards with portable arrays, *Eos Trans. AGU* **86**, 169–173, doi: [10.1029/2005EO170001](https://doi.org/10.1029/2005EO170001).
- Eaton, D. W., F. A. Darbyshire, R. L. Evans, H. Grütter, A. G. Jones, and X. Yuan (2009). The elusive lithosphere–asthenosphere boundary (LAB) beneath cratons, *Lithosphere* **109**, no. 1, 1–22.
- Eaton, D. W., S. Dineva, and R. Mereu (2006). Crustal thickness and V_P/V_S variations in the Grenville orogen (Ontario, Canada) from analysis of teleseismic receiver functions, *Tectonophysics* **420**, nos. 1/2, 223–238, doi: [10.1016/j.tecto.2006.01.023](https://doi.org/10.1016/j.tecto.2006.01.023).
- Ferreira, A. M. G., J. H. Woodhouse, K. Visser, and J. Trampert (2010). On the robustness of global radially anisotropic surface wave tomography, *J. Geophys. Res.* **115**, no. B4, doi: [10.1029/2009JB006716](https://doi.org/10.1029/2009JB006716).
- Frederiksen, A. W., M. G. Bostock, and J. F. Cassidy (2001). S -wave velocity structure of the Canadian upper mantle, *Phys. Earth Planet. In.* **124**, no. 3, 175–191.
- Hales, A. L. (1969). A seismic discontinuity in the lithosphere, *Earth Planet. Sci. Lett.* **7**, 44–46.
- Helffrich, G. (2006). Extended-time multitaper frequency domain cross-correlation receiver-function estimation, *Bull. Seismol. Soc. Am.* **96**, no. 1, 344–347, doi: [10.1785/0120050098](https://doi.org/10.1785/0120050098).
- Kao, H., Y. Behr, C. A. Currie, R. D. Hyndman, J. Townend, F.-C. Lin, M. H. Ritzwoller, S.-J. Shan, and J. He (2013). Ambient seismic noise tomography of Canada and adjacent regions: Part I. Crustal structures, *J. Geophys. Res.* **118**, 1–23, doi: [10.1002/2013JB010535](https://doi.org/10.1002/2013JB010535).
- Kennett, B. L. N., E. R. Engdahl, and R. Buland (1995). Constraints on seismic velocities in the Earth from traveltimes, *Geophys. J. Int.* **122**, no. 1, 108–124.
- Laske, G., G. Masters, Z. Ma, and M. E. Pasyanos (2013). Update on CRUST1.0—A 1-degree global model of Earth's crust, *Geophys. Res. Abstr.* **15**, Abstract EGU2013-2658, <http://igppweb.ucsd.edu/~gabi/rem.html> (last accessed September 2013).
- Lebedev, S., J. Boonen, and J. Trampert (2009). Seismic structure of Precambrian lithosphere: New constraints from broad-band surface-wave dispersion, *Lithosphere* **109**, 96–111, doi: [10.1016/j.lithos.2008.06.010](https://doi.org/10.1016/j.lithos.2008.06.010).
- Levin, V., and J. Park (2000). Shear zones in the Proterozoic lithosphere of the Arabian shield and the nature of the Hales discontinuity, *Tectonophysics* **323**, nos. 3/4, 131–148.
- Marone, F., and B. Romanowicz (2007). Non-linear crustal corrections in high-resolution regional waveform seismic tomography, *Geophys. J. Int.* **170**, no. 1, 460–467, doi: [10.1111/j.1365-246X.2007.03399.x](https://doi.org/10.1111/j.1365-246X.2007.03399.x).
- Mooney, W. D., G. Laske, and T. G. Masters (1998). Crust5.1: A global model at 5° by 5°, *J. Geophys. Res.* **103**, no. B1, 727–747, doi: [10.1029/97JB02122](https://doi.org/10.1029/97JB02122).
- Nair, S. K., S. S. Gao, K. H. Liu, and P. G. Silver (2006). Southern African crustal evolution and composition: Constraints from receiver function studies, *J. Geophys. Res.* **111**, no. B02304, doi: [10.1029/2005JB003802](https://doi.org/10.1029/2005JB003802).
- Panning, M. P., V. Lekić, and B. A. Romanowicz (2010). Importance of crustal corrections in the development of a new global model of radial anisotropy, *J. Geophys. Res.* **115**, no. B12, doi: [10.1029/2010JB007520](https://doi.org/10.1029/2010JB007520).
- Pawlak, A., D. W. Eaton, I. D. Bastow, J.-M. Kendall, G. Helffrich, J. Wookey, and D. B. Snyder (2011). Crustal structure beneath Hudson Bay from ambient-noise tomography: Implications for basin formation, *Geophys. J. Int.* **184**, no. 1, 65–82, doi: [10.1111/j.1365-246X.2010.04828.x](https://doi.org/10.1111/j.1365-246X.2010.04828.x).

- Perry, H. K. C., D. W. Eaton, and A. M. Forte (2002). LITH5.0: A revised crustal model for Canada based on lithoprobe results, *Geophys. J. Int.* **150**, no. 1, 285–294, doi: [10.1046/j.1365-246X.2002.01712.x](https://doi.org/10.1046/j.1365-246X.2002.01712.x).
- Postlethwaite, B., M. G. Bostock, N. I. Christensen, and D. B. Snyder (2014). Seismic velocities and composition of the Canadian crust, *Tectonophysics* **633**, 256–267, doi: [10.1016/j.tecto.2014.07.024](https://doi.org/10.1016/j.tecto.2014.07.024).
- Ritsema, J., H. J. van Heijst, and J. H. Woodhouse (2004). Global transition zone tomography, *J. Geophys. Res.* **109**, no. B2, B02302, doi: [10.1029/2003JB002610](https://doi.org/10.1029/2003JB002610).
- Steffen, R., D. W. Eaton, and P. Wu (2012). Moment tensors, state of stress and their relation to post-glacial rebound in northeastern Canada, *Geophys. J. Int.* doi: [10.1111/j.1365-246X.2012.05452.x](https://doi.org/10.1111/j.1365-246X.2012.05452.x).
- Tesauro, M., M. K. Kaban, W. D. Mooney, and S. Cloetingh (2014). NACr14: A 3D model for the crustal structure of the North American continent, *Tectonophysics* **631**, 65–86, doi: [10.1016/j.tecto.2014.04.016](https://doi.org/10.1016/j.tecto.2014.04.016).
- Thompson, D. A., I. D. Bastow, G. Helffrich, J.-M. Kendall, J. Wookey, D. B. Snyder, and D. W. Eaton (2010). Precambrian crustal evolution: Seismic constraints from the Canadian shield, *Earth Planet. Sci. Lett.* **297**, nos. 3/4, 655–666, doi: [10.1016/j.epsl.2010.07.021](https://doi.org/10.1016/j.epsl.2010.07.021).
- Thompson, D. A., G. Helffrich, I. D. Bastow, J.-M. Kendall, J. Wookey, D. W. Eaton, and D. B. Snyder (2011). Implications of a simple mantle transition zone beneath cratonic North America, *Earth Planet. Sci. Lett.* **312**, nos. 1/2, 28–36, doi: [10.1016/j.epsl.2011.09.037](https://doi.org/10.1016/j.epsl.2011.09.037).
- Waldhauser, F., R. Lippitsch, E. Kissling, and J. Ansorge (2002). High-resolution teleseismic tomography of upper-mantle structure using an *a priori* three-dimensional crustal model, *Geophys. J. Int.* **150**, no. 2, 403–414.
- Wessel, P., and W. H. F. Smith (1995). New version of the Generic Mapping Tools released, *Eos Trans. AGU* **76**, no. 33, 329.
- Zhu, L., and H. Kanamori (2000). Moho depth variation in southern California from teleseismic receiver functions, *J. Geophys. Res.* **105**, 2969–2980.

D. A. Thompson^{1,2}
School of Geosciences
King's College
University of Aberdeen
Aberdeen AB24 3UE, United Kingdom
david.thompson@abdn.ac.uk

J.-M. Kendall
J. Wookey
School of Earth Sciences
University of Bristol
Wills Memorial Building
Queen's Road
Bristol BS8 1RJ, United Kingdom

*G. R. Helffrich*¹
Earth and Life Science Institute
Tokyo Institute of Technology
2-12-1-IE-1 Ookayama
Meguro-ku
Tokyo 152-8550, Japan

I. D. Bastow
Department of Earth Science and Engineering
Imperial College London
South Kensington Campus
London SW7 2AZ, United Kingdom

D. B. Snyder
Geological Survey of Canada
Natural Resources Canada
615 Booth Street
Ottawa, Ontario
Canada K1A 0E9

Published Online 29 July 2015

¹ Also at School of Earth and Environment, University of Leeds, Leeds LS2 9JT, United Kingdom.

² Also at School of Earth Sciences, University of Bristol, Wills Memorial Building, Queen's Road, Bristol BS8 1RJ, United Kingdom.